LA-UR-01-4768
Approved for public release;
distribution is unlimited.

Title: **An Integrated Solid-State Optical Device with High-Speed Scanning, Variable Focusing, and Frequency-Doubling Capabilities**

Author(s): Quanxi Jia, Kevin T. Gahagan, Venkatraman Gopalan, Joanna L. Casson, Terence E. Mitchell, and Jeanne M. Robinson

Submitted to:

An Integrated Solid-State Optical Device with High-Speed Scanning, Variable Focusing, and Frequency-Doubling Capabilities

Quanxi Jia* (MST-STC), Kevin T. Gahagan (C-6),
Venkatraman Gopalan (Pennsylvania State University), Joanna L. Casson (C-6),
Terence E. Mitchell (MST-10), and Jeanne M. Robinson (C-6)

Abstract

The incredibly rich range of linear and non-linear optical properties exhibited by ferroelectrics such as lithium tantalate has given us the ability to perform the basic operations with light, such as high speed scanning, focusing and frequency conversion, all in one material. These devices depend critically on the ability to manipulate the ferroelectric domain structure on a micron scale. The goal of this project is to develop the first of its kind of integrated device that will act as the basis for a new generation of integrated solid state optical devices incorporating further functions. The devices including electro-optic lenses and scanners have been successfully integrated on a single-crystal ferroelectric lithium-tantalate wafer. We envision this as the first step towards the development of a comprehensive solid state platform with various optical components.

Background and Research Objectives

The future in data storage and communications is heading towards the optical regime. Optical data fusion networks with an aggregate throughput of about 1 Terabit/sec will be used to transmit audio and video data in real time facilitating teleconferencing, telemedicine, education, research and defense communications [1, 2]. The popularity of CD-ROMs in personal computers demonstrates the importance of optical recording for data distribution and archiving. Above 1Gb, the cost of the medium begins to dominate, at which point optical storage becomes the more cost-effective technology as compared to magnetic data storage [3].

With the emergence of optical data processing as a choice alternative, two fundamental thrusts can be identified. First, we need to manipulate light to do operations presently performed with electrons and magnetic media. Secondly, we need to progress [1]from bulk optics and benches to miniaturized solid state optical elements and their planar integration on a wafer. Thus, there is need for a versatile material platform, or a solid state

bench, which is capable of integrating a number of diverse optical components on one wafer, much like what silicon is to the electronic industry today.

Ferroelectrics offer just such a platform due to their incredibly rich array of linear and non-linear phenomena. The polarization, P, in a ferroelectric can be written as a function of electric field E as,

$$P = P_s + \chi^{(1)}E + \chi^{(2)}E^2 + \chi^{(3)}E^3 + \text{.....}$$

Thus we can integrate non-volatile ferroelectric memory elements, piezoelectric transducers and pyroelectric detectors (all arising from the spontaneous polarization, P_s) with optical waveguides, dispersion gratings and mirrors (arising from the first order term, $\chi^{(1)}$), with variable focus lenses, high speed scanners and modulators, and second harmonic generators (arising from the second order term $\chi^{(2)}$), with holographic storage elements and phase conjugate mirrors (arising from the third order term, $\chi^{(3)}$) and so on.

The critical element in the fabrication of these devices is the ability to microengineer ferroelectric domains. This is illustrated by the schematic of an integrated solid state optical head shown in Fig. 1 initially proposed to be developed on a ferroelectric lithium-tantalate wafer. The head provides a compact blue laser source, which can be focused and scanned at frequencies approaching GHz, all on a chip about 10mm x 20mm in size. Such a head has advantages [4] over conventional read/write optical heads in that halving the wavelength of light used for storage quadruples the storage density, it is compact with no moving parts, power consumption is low, and the high speed scanning ability significantly improves track access time.

This proposed integrated optical head consists of three parts: A blue light source based on second harmonic generation (SHG), electro-optic lenses and an electro-optic scanner. The second harmonic generator upconverts the frequency of an input infrared laser (e.g. 840 nm wavelength) into blue light (at 420 nm), which is then collimated by applying an electric field across electro-optic lenses, and finally passed through an electro-optic scanner which can raster the beam in one dimension laterally with the application of a high frequency ac field across it. The primary advantage here of using SHG for frequency conversion and electro-optics for scanning and lensing is that these technologies are naturally integrable on the same material platform. A further advantage of SHG using ferroelectrics as compared to wide-band gap semiconductors like GaN [5] or doped glasses [6] is the ease of tuning the blue wavelength by changing the period of the domain grating. Electro-optics offers the capability of approaching scanning speeds of a GHz in contrast to mechanical or acousto-optic scanners (MHz).

The core idea of this project is to develop a solid state optical bench using ferroelectric wafers and films towards demonstrating prototypical integrated devices for optical data storage and communications. We proceed towards this vision in two steps. First, we will demonstrate individual solid state optical components that perform basic functions with light, namely focusing, scanning, and frequency conversion. Specifically, we will design, fabricate and test the following components on lithium tantalate ferroelectric wafers: scanners, lenses, and frequency converters. This step will be strongly coupled to basic studies on the understanding of domain nucleation and growth mechanisms in ferroelectrics. Finally, we will demonstrate an integrated optical device, a high-speed optical scanner with variable focusing ability, on wafer as described in Fig. 1. We were able to accomplish most of the initially proposed tasks but integrating a blue light source on a single wafer due to the funding cutting in the final year of the project.

Importance to LANL's Science and Technology Base and National R&D Needs

This is the first step towards the development of a comprehensive solid state platform with various optical components such as lenses, scanners, frequency converters, modulators, gratings, mirrors, detectors, and storage elements that can enable any integrated solid state device to be designed and fabricated for diverse applications. The success of this program will depend on fundamental understanding of real-time nucleation and growth dynamics of domains in ferroelectrics, such as mobility of domain walls under an external field, stabilization mechanisms for domains, the structure of 180° domain walls, and the effect of chemical doping and radiation exposure on the dynamics of domains. The fundamental understanding of domains in ferroelectrics will also lead to the development of nanosize nonvolatile ferroelectric memories.

Scientific Approach and Accomplishments

The following just outlines three significant aspects of the project though tremendous progress has been made in this program (see the publication list – 18 refereed articles).

A. Device Modeling and Design

We have employed classical optics complemented by numerical simulation techniques such as Beam Propagation Method (BPM [7]) for the design of individual optical components, and their integration. The BPM is a powerful numerical technique to predict the phase distortions of a field $E(x,y,z)$ propagating in the z direction through a medium with variations in refractive index, $n(x, y, z)$. An initial field $E(x,y,0)$ is Fourier

decomposed and each propagation vector k, is propagated through a thin slice of the medium. The resulting distortions in phase are recovered by inverse Fourier transform of the field into real space. This process is cumulatively repeated over many slices as the beam propagates through the medium.

The following shows one example of optimization principles applied to the design of the scanner portion of the device. Here, we have followed the derivation presented by Chiu *et al.* [8] to describe an idealized horn shaped scanner with a slight modification. Lotspeich [9] has shown that the deflection angle from a single prism may be approximated by

$$\theta = n_0^2 r_{33} E \frac{L}{D}$$

where r_{33} is the electro-optic coefficient, L is the length, and D is the width of the device. A horn-shaped scanner follows the principle that each successive prism is just wide enough to accommodate the deflected beam. However, as the scanner widens toward the end of the horn, the additional deflection imparted by each successive prism is diminished. We have proposed to improve the device performance by splitting the prisms toward the end of the horn into pairs of prisms of equal width and approximately half the width of the original horn (see Figure 2). By including the split in the scanner as much as a 15 percent increase in the overall deflection angle is obtained compared with a conventional horn-shaped scanner of the same length and entrance aperture. The penalty paid for this increased angular range is the introduction of a small amount of distortion to the beam when the scanner is operated at low voltages (i.e. when the beam interacts with both sets of prisms in the split region). The operation of the integrated lens/scanner device was modeled using a one-dimensional fast Fourier-transform beam propagation method [10,11]. Figure 2 shows a simulation of a 4 μm input beam being collimated by the lens, then deflected through an angle of 10°. Figure 3 plots the result of the measurements yielding an angular dependence of 36.5 mrad/kV. This is in good agreement with the theoretical model of our system, computed from BPM simulations.

B. Experimental Methodology

We have focused on lithium-tantalate for the following reasons: (a) it has excellent non-linear optical properties (r_{33} = 21 pm/V). (b) it is available as high quality single crystal wafers at low cost. (c) Single crystal, single domain thin films of these materials

with low waveguiding losses can be synthesized. (d) 180° domains can be imaged easily by optical probes.

We have used lithographically defined chemical patterning by proton indiffusion combined with external electric field application to manipulate the domain structure. In this study, we, for the first time, have carried out real-time studies of nucleation and growth of 180 degree ferroelectric domains in congruent lithium-tantalate under an external electric field using Electro-Optic Imaging Microscopy (EOIM). Figure 4 shows a series of frames obtained from the EOIM data. Only a selective collage of frames is shown in Fig. 4 although we could extract 30 frames per second from the video from the start of the voltage pulse to the end of domain reversal process. If the step voltage was applied at time t = 0, the first frame (a) in Fig. 4 corresponds to t = 30 sec. Every successive frame is spaced by 15 sec. The final frame is Fig. 4(o) and corresponds to t = 240 s. The polarization axis is normal to the plane of image. The 180° domains nucleate and grow in the form of triangular domains with domain walls perpendicular to the mirror plane (for example domains I, II, III, IV shown in Figs. 4(c) and (d)). The crystallographic *y*-axis corresponds to $[1\bar{1}00]$ and lies in the mirror plane. Eventually, the domains merge sideways and form a merged domain front like the domain V, VI, and VII indicated in Fig. 4(e) and (g). The arrows indicate the location and direction of sideways velocity measurement of these fronts. We observed that the measured wall velocities are an order of magnitude higher than those reported before using ex-situ techniques. Merger of growing domain forms serrated fronts that show a further order of magnitude increase in wall velocity. For example, domain wall velocity of independently growing domains shows an average steady state velocity of 4.6 ± 2 μm/s. On the other hand, merged domain fronts show an average steady state velocity of 63 ± 11 μm/s.

C. Integration Issues

We have successfully demonstrated the integration of an independently controlled high-power electro-optic lens and large-angle scanner on a single-crystal lithium-tantalate wafer. The lens is capable of collimating light exiting from waveguides with diameters ranging from 4 - 40 μm. The collimated light is then deflected over an angular range of nearly 20° by the independently controlled deflector. This scan range is nearly five times the previously reported highest range for a continuous scanning electro-optic deflector and may provide a faster, more mechanically robust alternative to galvanometer type and other

mechanical scanning systems for some applications. As shown in Figure 5, excellent beam quality is maintained over a range of almost 140 mrad. Distortion from the split-horn portion of the scanner (not shown) was found to be minimal within ± 100 V of zero and above ± 400 V.

Publications

1. V. Gopalan, T. E. Mitchell, K. E. Sickafus, and Q. X. Jia, "Real-time study of kinetics of 180 degree domains in congruent $LiTaO_3$ under an external field," Integrated Ferroelectrics **22**, 925 (1998).

2. V. Gopalan and T. E. Mitchell, "Wall velocities, switching times, and stabilization mechanism of 180 domains in $LiTaO_3$ crystals," J. Appl. Phys. **83**, 941 (1998).

3. V. Gopalan, T. E. Mitchell, Y. Furukawa, K. Kitamura, "The role of nonstoichiometry in 180 domain switching of $LiNbO_3$ crystals," Appl. Phys. Lett. **72**, 1981 (1998).

4. V. Gopalan, T. E. Mitchell, Q. X. Jia, J. M. Robinson, M. J. Kawas, T. E. Schlesinger, D. D. Stancil, "Ferroelectrics as a versatile solid state platform for integrated optics," Integrated Ferroelectrics **22**, 985 (1998).

5. K. Kitamura, N. Furukawa, K. Niwa, V. Gopalan, T. E. Mitchell, "Crystal growth and low-field 180 degree domain switching characteristics of stoichiometric $LiTaO_3$," Appl. Phys. Lett. **73**, 3073 (1998).

6. V. Gopalan, K. E. Sicafus, T. E. Mitchell, "Switching kinetics of 180 degree domains in congruent $LiNbO_3$ and $LiTaO_3$ crystals," Solid State Communications **109**, 111 (1999).

7. K. T. Gahagan, V. Gopalan, J. M. Robinson, Q. X. Jia, T. E. Mitchell, "Integrated electro-optic lens/scanner in $LiTaO_3$ single crystal," Applied Optics **38**, 1186 (1999).

8. V. Gopalan and T. E. Mitchell, "In-situ video observation of 180 degree domain switching in $LiTaO_3$ by electro-optic imaging microscopy," J. Appl. Phys. **85**, 2304 (1999).

9. V. Gopalan, S. S. A. Gerstl, A. Itagi, Q. X. Jia, T. E. Mitchell, T. E. Schlesinger, D. D. Stancil, "Mobility of 180° domain walls in congruent $LiTaO_3$ measured using in-situ electro-optic imaging microscopy," J. Appl. Phys. **86**, 1638 (1999).

10. K. T. Gahagan, V. Gopalan, J. M. Robinson, Q. X. Jia, T. E. Mitchell, M. J. Kawas, T. E. Schlesinger, D. D. Stancil, " Fabrication and characterization of high-speed integrated electro-optic lens and scanner devices," Proceedings of the SPIE, **3620**, 374 (1999).

11. Y. Gim, K. T. Gahagan, C. Kwon, M. Hawley, V. Gopalan, J. M. Robinson, T. E. Mitchell, and Q. X. Jia, "Growth of $LiNbO_3$ films on single crystal sapphire substrates using pulsed laser deposition," Integrated Ferroelectrics **25**, 431 (1999).

12. V. Gopalan, K. T. Gahagan, M. Kawas, Q. X. Jia, J. M. Robinson, T. E. Mitchell, T. E. Schlesinger, D. D. Stancil, "Integration of electro-optic lenses and scanners on ferroelectric $LiTaO_3$," Integrated Ferroelectrics **25**, 371 (1999).

13. V. Gopalan, Q. X. Jia, T. E. Mitchell, "In-situ video observation of 180° domain kinetics in congruent $LiNbO_3$ crystals," Appl. Phys. Lett. **75**, 2482 (1999).

14. V. Gopalan, A. Itagi, S. Gerstl, P. Swart, Q. X. Jia, T. E. Mitchell, T. E. Schlesinger, D. D. Stancil, "Ferroelectric domain kinetics in congruent $LiTaO_3$," Integrated Ferroelectrics **27**, 1181 (1999).

15. C. C. Battle, S. Kim, V. Gopalan, K. Barkocy, M. C. Gupta, Q. X. Jia, and T. E. Mitchell, "Ferroelectric domain reversal in congruent $LiTaO_3$ crystals at elevated temperatures," Appl. Phys. Lett. **76**, 2436 (2000).

16. K. T. Gahagan, David A. Scrymgeour, Joanna L. Casson, J. M. Robinson, V. Gopalan, "Integrated high power electro-optic lens and large-angle deflector," submitted to Appl. Optics, Nov. 2000.

17. K. T. Gahagan, J. M. Robinson, J. L. Casson, V. Gopalan, D. A. Scrymgeour, "Integrated high power electrooptic lens/scanner for space-based platforms," submitted to SPIE Proceedings, July 10, 2000.

18. D. A. Scrymgeour, Y. Barad, V. Gopalan, K. T. Gahagan, J. M. Robinson, Q. X. Jia, T. E. Mitchell, "A large angle electro-optic scanner on $LiTaO_3$ fabricated by in-situ monitoring of ferroelectric domain microengineering," submitted to Appl. Optics, Sept. 2000.

References

[1] McMillen, G., Coathup, L., Lu, C-Y., "Application requirements for an all-optical network," Proc. Optical Fiber Commun., pp. 65, (1994).
[2] Snelling, R., "Broad-band communication networks," Proc. Optical Fiber Commun., pp.4, (1989).
[3] Asthana, P., "A long road to overnight success," IEEE Spectrum **31**, 60 (1994).
[4] Nishihara, H., Suhara, T., and Ura, S., "An Integrated Optic disc pickup device," J. Lightwave Technology **4**, 913 (1986).
[5] Nakamura, S., *High brightness blue/green LEDs and first III-V nitride based laser diodes*, Proc. SPIE **2693**, 43 (1996).
[6] Carrig, T. J., Cockroft, N. J., *Upconversion Processes in Yb-sensitized Tm-ZBLAN*, Proc. SPIE **2841**, 231 (1996).
[7] Feit, M. D., Fleck, J. A., "Calculation of dispersion in graded-index multimode fibers by a propagating-beam method," Appl. Optics **18**, 2843 (1979).
[8] Chiu, Y., Zou, J., Stancil, D. D., Schlesinger, T. E., "Shape-optimized electrooptic beam scanners: analysis, design, and simulation," J. Lightwave Tech. **17**, 108 (1999).
[9] Lotspeich, J. F., "Electro-optic light-beam deflection," IEEE Spectrum **5**, 45 (1968).
[10] Fleck, J. A., Morris, J. R., Feit, M. D., "Time-dependent propagation of high-energy laser-beams through atmosphere," Appl. Phys. **10**, 129 (1976).
[11] Feit, M. D., Fleck, J. A., "Light-propagation in graded-index optical fibers," Appl. Optics **17**, 3990 (1978).

Figure Captions

Figure 1: Proposed solid state integrated head for optical data storage on a ferroelectric wafer. The figure is not drawn to scale. The period of the SHG grating is ~3.6 μm, while the feature size of the lenses and deflectors are about 1mm.

Figure 2: BPM simulation of integrated device shown collimating a 4 μm beam with the lens, then deflecting through an angle of ~10°. From the superimposed ferroelectric domain boundaries (white lines), the split-horn design variation on a classical horn-shaped can be seen.

Figure 3: Measured deflection angle *vs*. applied voltage for scanner component of integrated device.

Figure 4: Selected video frames from in-situ recording of the nucleation and growth of 180° domains in congruent $LiTaO_3$ under an external field of 207.6 kV/cm (applied at time t = 0sec) using EOIM. Frame (a) corresponds to t = 30sec, and all successive frames [(b)-(o)] are 15 sec apart from each other. The polarization axis is normal to the plane of the figure (the *z*-plane) and the crystallographic *x* and *y* axes are marked. For independently growing domains (I, II, III, IV) and three merged domain fronts (V, VI, VII) for which domain mobilities were measured are labeled. The arrows in frames (e) and (g) indicate the location and direction of wall velocity measurement for the merged fronts V, VI, and VII.

Figure 5: Representative beam profiles as a function of applied voltage for selected voltage levels.

Figure 1

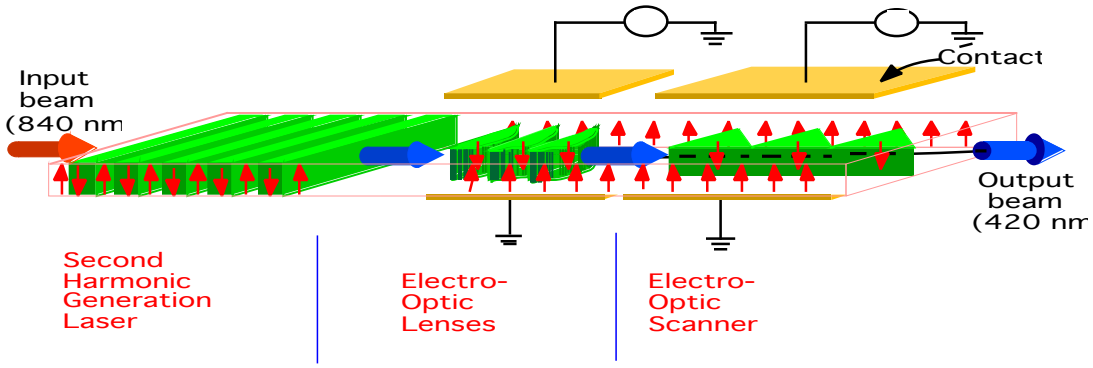
Input
beam
(840 nm
Contact
Output
beam
(420 nm
Second
Harmonic
Generation
Laser
Electro-
Optic
Lenses
Electro-
Optic
Scanner

Figure 2

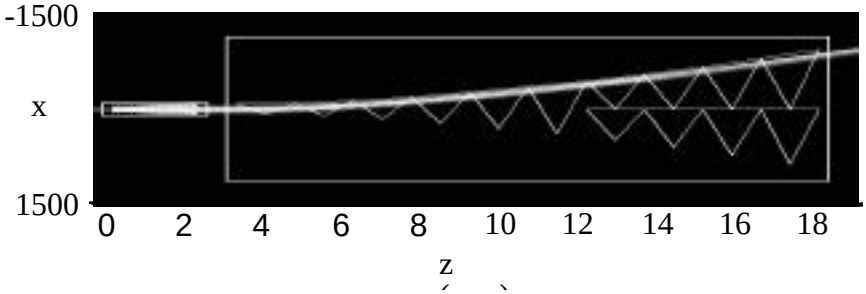

Figure 3

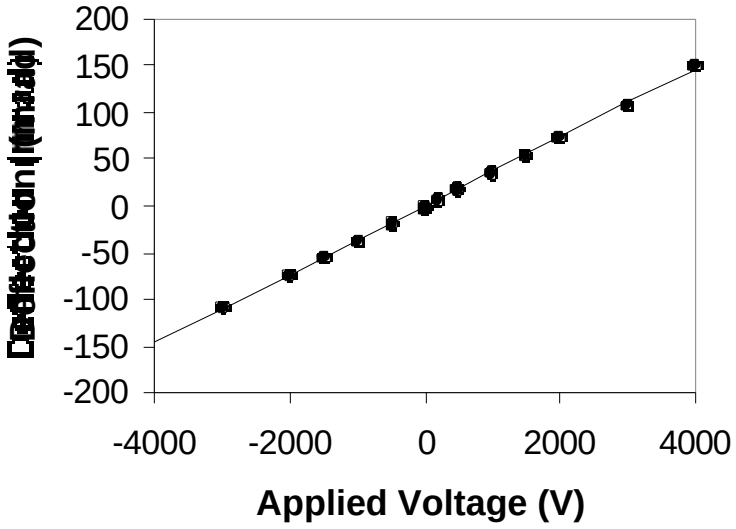
200
150
100
50
0
-50
-100
-150
-200
-4000
-2000
0
2000
4000
Applied Voltage (V)

Figure 4

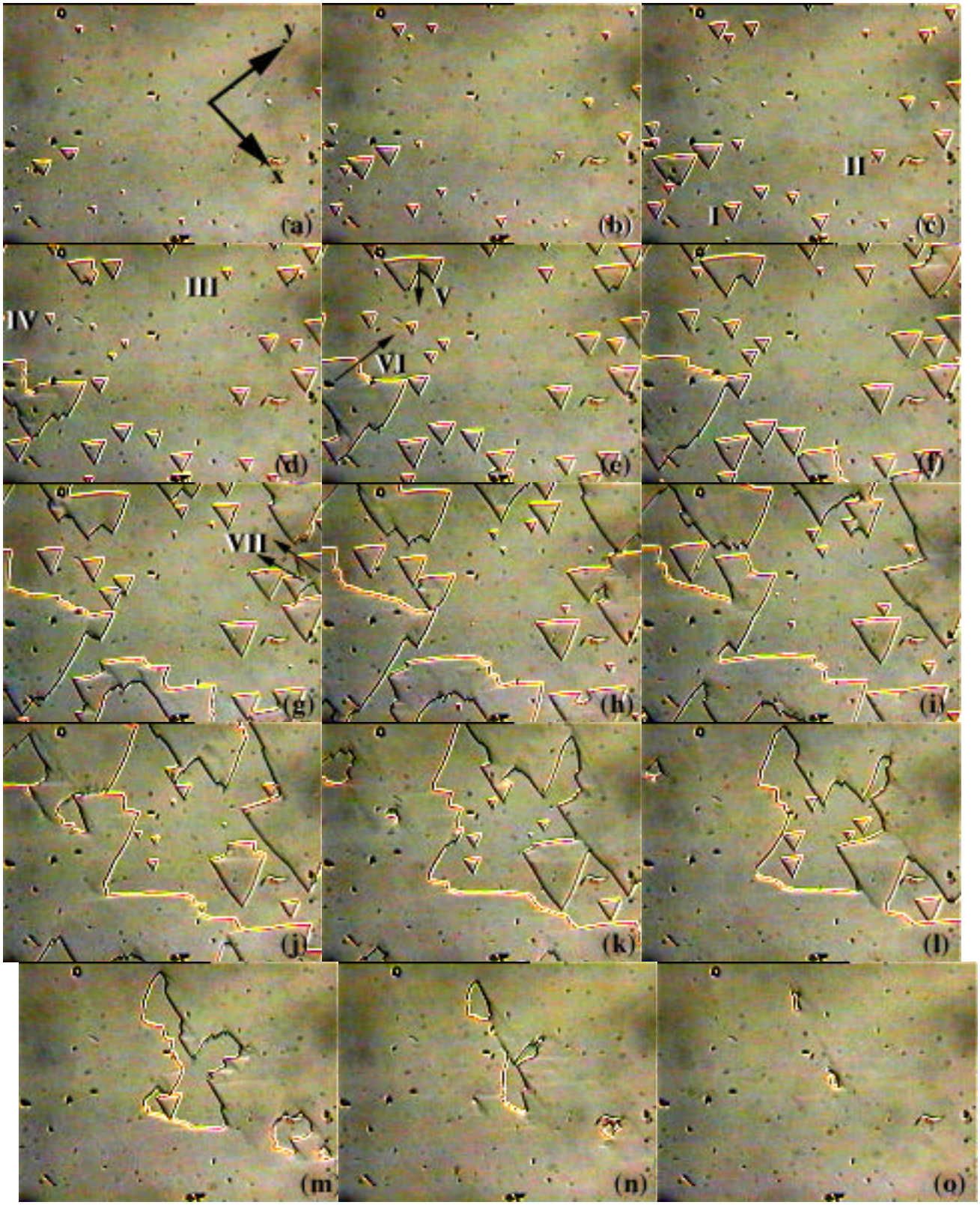

Figure 5

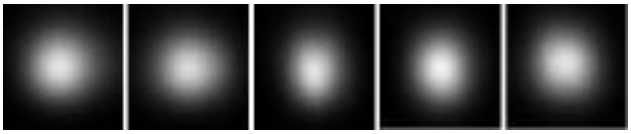

-1.9 V -1.2 V 0 V 1.2 V 1.9 V